


Cite this: *RSC Adv.*, 2020, 10, 35397

Core-shell magnetic mesoporous N-doped silica nanoparticles: solid base catalysts for the preparation of some arylpyrimido[4,5-*b*]quinoline diones under green conditions†

Shekofeh Neamani,^a Leila Moradi ^{*a} and Mingxuan Sun ^b

Nowadays, the application of solid base catalysts as a perfect replacement for homogenous basic catalysts has attracted the attention of researchers. In this study, core-shell magnetic mesoporous N-doped silica nanoparticles N(x wt%)-MSN, as a heterogeneous base catalyst, were synthesized. The N(x wt%)-MSN composite was fabricated by adding different amounts of diethanolamine as a source of nitrogen, besides using tetraethylorthosilicate as a precursor of silica. The as-prepared catalyst was employed efficiently for the synthesis of some arylpyrimido[4,5-*b*]quinoline-dione derivatives under green conditions. The highly efficient catalyst N(1.3 wt%)-MSN was characterized via XRD, FESEM, HRTEM, BET and XPS techniques, and the results of these analyses proved that the nitrogen was doped into the silica structure. Also, the results demonstrated the core-shell structure of the as-synthesized composite.

Received 28th July 2020
Accepted 31st August 2020

DOI: 10.1039/d0ra06546c

rsc.li/rsc-advances

Introduction

The development of new and efficient nanostructured base catalysts with accessible active sites is an important field in chemistry.^{1,2} Up to now, various types of heterogeneous solid base catalysts based on hydrotalcites,^{3,4} zeolites,⁴ basic ionic liquids⁴ and organic/inorganic hybrids⁵ have been reported. In this regard, use of mesoporous silica (with unique characteristics) as a support for the synthesis of heterogeneous basic catalysts has attracted much consideration.^{6–8} Some important properties of mesoporous silica include high surface area, thermal stability, narrow pore size distribution, controllable porosity and morphology.^{9–13} The surface modification of mesoporous silica frameworks with basic characteristic fabricated using basic organosilane reagents has been reported.^{14,15} Irreversible participation of the anchored organic species in the reaction and also, structural destruction at elevated temperatures in air atmosphere or in the presence of oxidative agents limit the application of such catalysts.^{15,16} Doping nitrogen in the flexible silicate framework and placing it in the form of bridged Si–NH–Si groups is a novel technique for incorporating basic sites into silica nanoparticles.^{17–19} These N-doped catalysts show appropriate basic activity similar to the typical base catalysts in reactions. The N-doped silica could be obtained by

passing ammonia gas on the surface of mesoporous silica under harsh reaction conditions. Doping nitrogen by this technique could be performed at high temperatures, approximately 1173–1423 K; however, such methods require high-tech tools.^{17,18} Another less developed method for nitrogen doping in different frameworks is using a precursor containing nitrogen atoms. In this method, during the synthesis of the intended framework, a precursor containing nitrogen atoms is added to the mixture. Then, the mixture is calcined in a furnace to produce N-doped structures. In 2019, Ghiaci *et al.* prepared nitrogen-doped carbon networks by the pyrolysis of salen complexes in the argon atmosphere.²⁰ Caruso *et al.* in 2016 synthesized porous nitrogen-modified titania (N-TiO₂) using diethanolamine (DEA) and titanium(IV) butoxide. The prepared N-TiO₂ was applied for dye removal at room temperature.²¹ In our previous work in 2020, we reported the preparation of nitrogen-doped silica materials using DEA as a precursor of nitrogen in the silica framework. The prepared catalyst was applied as a basic heterogeneous catalyst for the synthesis of some dihydropyridine derivatives.¹

Recently, core-shell structures have attracted considerable attention due to their great applications as a catalyst in reactions. Unlike typical catalysts, the core-shell materials can incorporate several functions into a system for particular uses. Between the core-shell catalysts, composites containing magnetic cores have numerous applications such as selective separation, synthesis of fine chemicals, drug delivery, chromatography, and biological sensors.^{22,23}

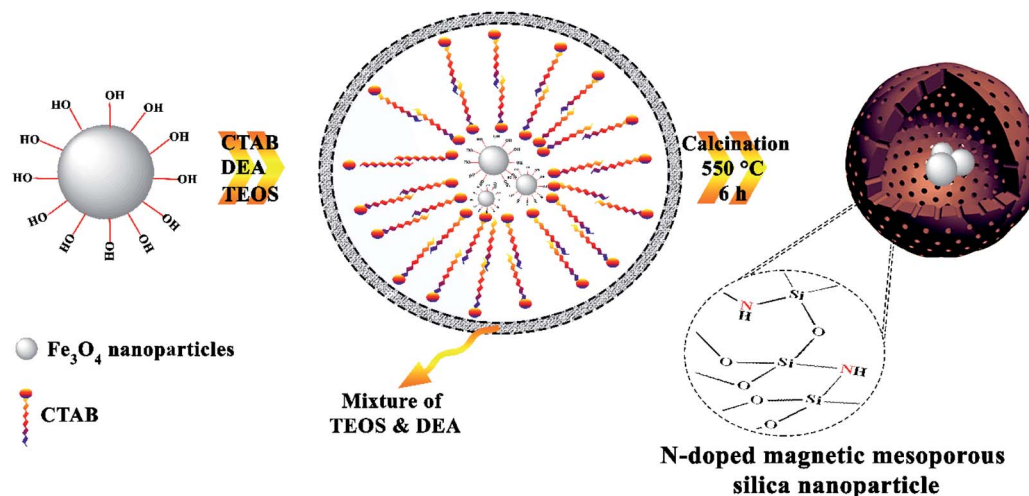
In this study, to prepare the magnetic nitrogen-doped silica core-shells, we used DEA as a source of nitrogen, and tetraethyl

^aDepartment of Organic Chemistry, Faculty of Chemistry, University of Kashan, P.O. Box 8731753153, Kashan, I. R. Iran. E-mail: l_moradi@kashanu.ac.ir

^bSchool of Materials Engineering, Shanghai University of Engineering Science, China

† Electronic supplementary information (ESI) available. See DOI: 10.1039/d0ra06546c





Scheme 1 Synthesis of the N(x wt%)-MSN composite.

orthosilicate (TEOS) for the *in situ* synthesis of N-doped silica shell on the magnetic cores. The as-prepared catalyst was used as a strong heterogeneous base catalyst for the synthesis of some quinoline derivatives under green conditions [4,5-*b*]. The quinoline derivatives are abundant in nature and exhibit numerous biological properties such as antitumor, antimalarial, antibacterial, anthelmintic, anti-inflammatory, antiplatelet and antiasthmatic.^{24–30}

Results and discussion

Catalyst characterization

In this work, magnetic N-doped silica nanoparticles were prepared and their efficiency was investigated in the synthesis of arylpyrimido[4,5-*b*]quinoline dione derivatives. Scheme 1 shows the preparation method of the core-shell magnetic mesoporous N-doped silica nanoparticles or N(x wt%)-MSN in which *x* represents the amount of doped nitrogen in the final structure. During the preparation of mesoporous silica nanoparticles (using TEOS precursor and different amounts of DEA), the DEA molecules are trapped into the silica frameworks. Calcining the as-obtained samples at 550°C resulted in the doping of different amounts of doped nitrogen atoms into the structure of silica magnetic nanoparticles (Scheme 1).

The amount of doped nitrogen in the as-prepared catalysts was investigated by an elemental analysis. According to the obtained data, when 0.5, 1.0 and 1.5 mL of DEA were used, 0.6, 1.3 and 1.7 wt% of N atoms were doped, respectively, in the mesoporous silica nanostructures. Based on the experimental results from the synthesis of some arylpyrimido[4,5-*b*]quinoline-dione derivatives, the catalyst containing 1.0 mL of the DEA precursor (N(1.3 wt%)-MSN) shows the best performance as a heterogeneous catalyst. Accordingly, the structural properties of N(1.3 wt%)-MSN has been discussed further.

The morphology of the N(1.3 wt%)-MSN catalyst was investigated *via* FESEM (Fig. 1). According to the results, generally, two different types of morphologies (spherical and amorphous aggregates) are observed for the as-synthesized catalyst. The presence of aggregated structures can be related to the increased hydrolysis rate of the silica precursor in the reaction medium. In fact, the presence of DEA during the synthesis of silica nanoparticles causes an effect on the hydrolysis rate of silica precursors, leading to amorphous silica with spherical shapes.

The HRTEM analysis of N(1.3 wt%)-MSN is presented in Fig. 2. It can be seen that the obtained images confirm the core-shell morphology of the magnetic mesoporous N-doped silica nanostructures. Moreover, it is clear that magnetic

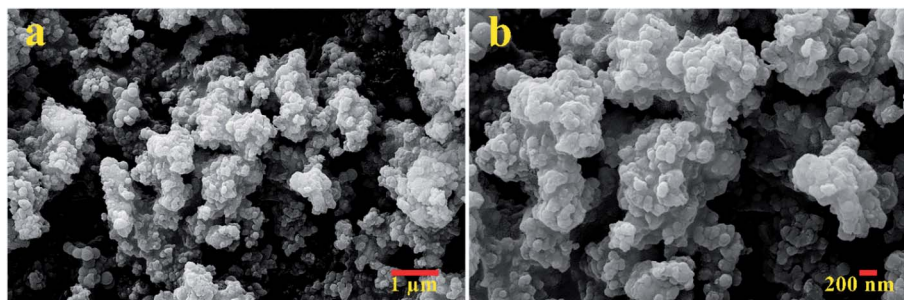


Fig. 1 FESEM of N(1.3 wt%)-MSN.



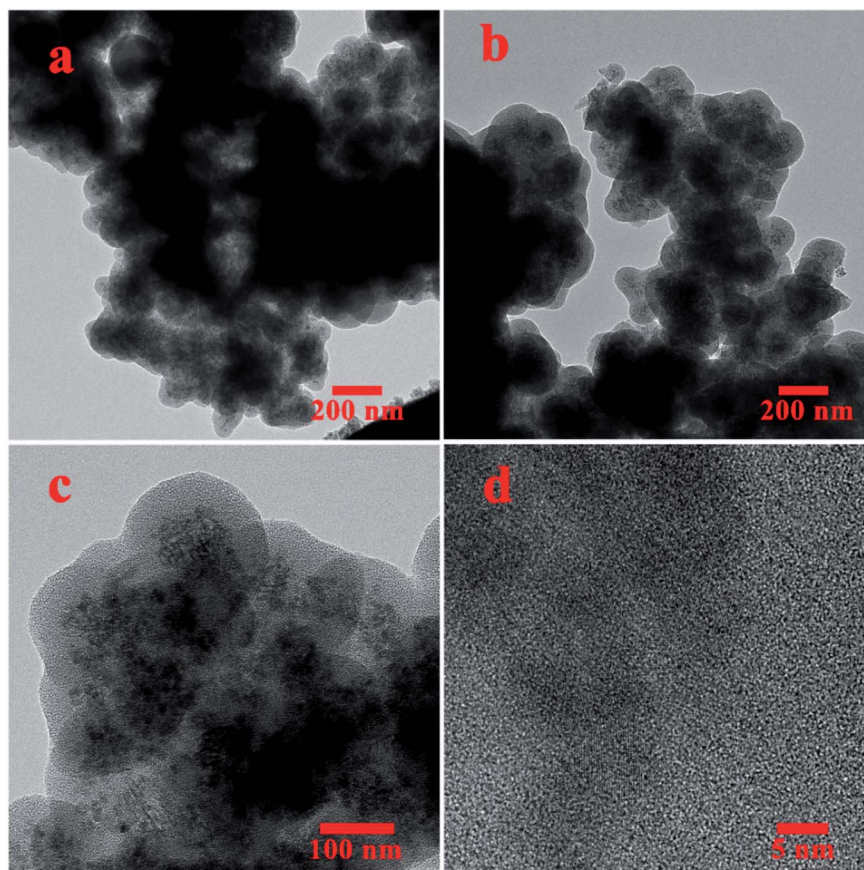


Fig. 2 HRTEM analysis of synthesized N(1.3 wt%)-MSN.

nanoparticles are well trapped within the mesoporous silica spherical shells to form core-shell structures.

To investigate the crystallinity of the structure of the magnetic N-doped nanoparticles, powder X-ray diffraction (XRD) patterns of MSN and N(1.3 wt%)-MSN were obtained. As shown in Fig. 3, a broad peak around $2\theta \approx 21-26^\circ$, representing

an amorphous silica structure both in MSN and N(1.3 wt%)-MSN can be seen. The amorphous peak in the N-doped mesoporous silica nanoparticle showed a shift to a lower 2θ , compared to that in mesoporous silica nanoparticles. This proved a change in the morphology and d -spacing of the silica structure, which is a result of doping nitrogen into the silica

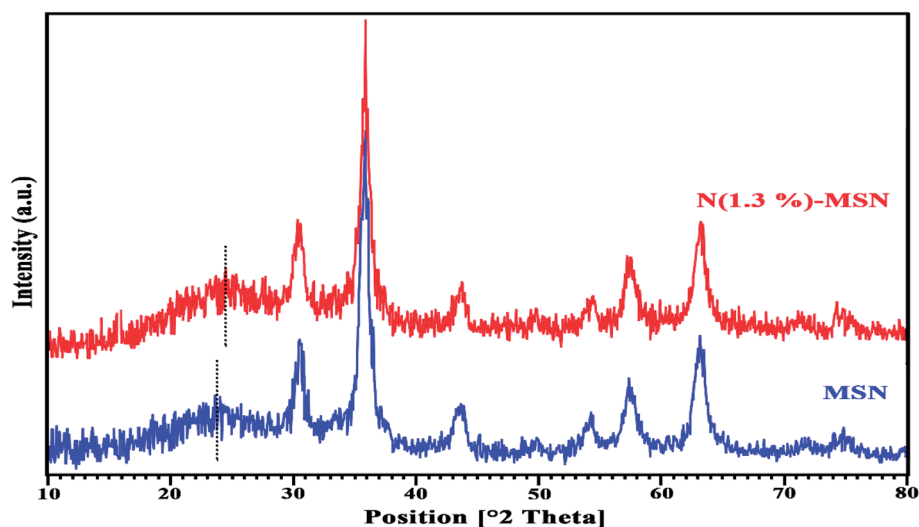


Fig. 3 XRD patterns of the as-synthesized N(1.3 wt%)-MSN and MSN.

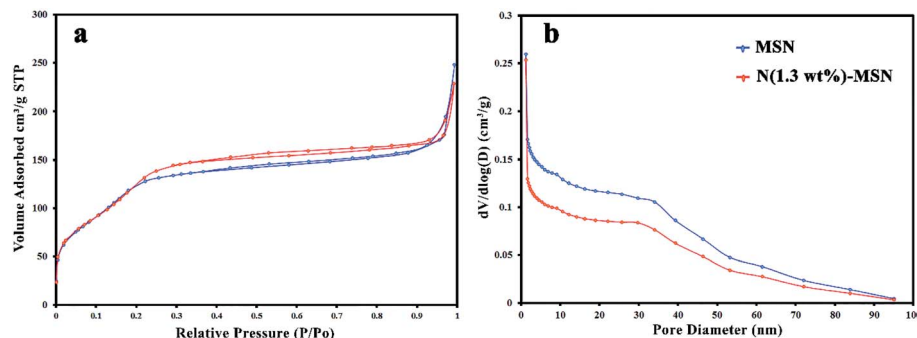


Fig. 4 (a) Nitrogen adsorption-desorption isotherms of MSN and N(1.3 wt%)-MSN, (b) BJH plots of MSN and N(1.3 wt%)-MSN.

frameworks. The other peaks in the XRD patterns of MSN and N(1.3 wt%)-MSN were associated with Fe_3O_4 nanoparticles and the presence of some Fe_2O_3 nanoparticles. The over oxidation of Fe_3O_4 nanoparticles in the furnace caused the formation of some Fe_2O_3 nanoparticles.^{18,31,32}

In Fig. 4, nitrogen adsorption-desorption isotherms of MSN and N(1.3 wt%)-MSN nanocomposite, and BJH plots of them are compared. According to the obtained results, MSN shows a surface area of $361 \text{ m}^2 \text{ g}^{-1}$ with a total pore volume of $0.37 \text{ cm}^3 \text{ g}^{-1}$ and a mean pore diameter of 4.1 nm. However, N(1.3 wt%)-MSN showed a surface area of $387 \text{ m}^2 \text{ g}^{-1}$, a total pore volume of $0.35 \text{ cm}^3 \text{ g}^{-1}$ and a mean pore diameter of 3.6 nm. Consequently, the as-prepared N(1.3 wt%)-MSN composite had a higher surface area with a less mean pore diameter, which established the presence of nitrogen atoms in the final mesoporous silica structure.

Finally, to establish the nitrogen doping into the silica frameworks, X-ray photoelectron spectroscopy was performed on the N(1.3 wt%)-MSN composite (Fig. 5). The deconvolution of the Si 2p spectrum reveals two main peaks at 103.3 and 104.5 eV related to Si-N and Si-O bonds, respectively (Fig. 5a). The presence of Si-N bonds successfully proved the doping of nitrogen atoms in silica frameworks. In Fig. 5b, the obtained N 1s spectrum of N(1.3 wt%)-MSN composite is shown. Due to the

low concentration of nitrogen atoms in the N(1.3 wt%)-MSN composite, the deconvolution of it does not offer specific information about the oxidation states of nitrogen. However, it is clear that the Si-N-H bond at 400.2 eV has the maximum involvement.³²⁻³⁵

Catalytic performance

To obtain proper and green conditions for the synthesis of some arylpyrimido[4,5-*b*]quinoline derivatives, the reaction of barbituric acid, 3-nitrobenzaldehyde and 4-methoxy aniline was considered as a model reaction. All of the effective factors including the solvent, catalyst and temperatures were studied for determining the optimized conditions. In this regard, the efficiency of the as-synthesized solid base catalysts and some of the homogeneous basic catalysts in different solvents was investigated. The model reaction was accomplished in various solvents using some homogenous base catalysts.

Results from Table 1 show that when Et_3N or L-proline was used as a catalyst, the yield of the product was low (in various solvents), and there no product was formed when the reaction was performed under catalyst-free conditions (entry 1) and when MSN was used as a catalyst (entry 14). The study on the relationship between the wt% of N atoms doped in the catalyst structure and catalyst efficiency was performed in reactions

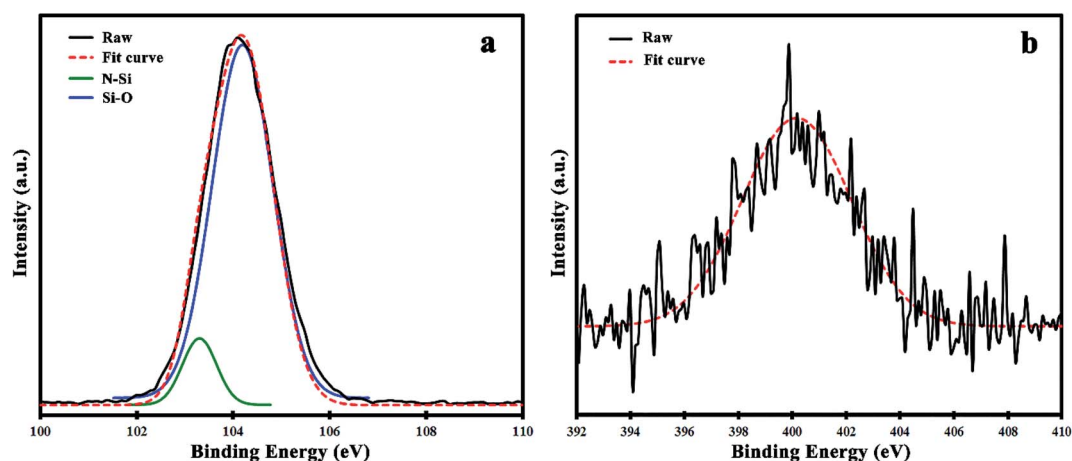
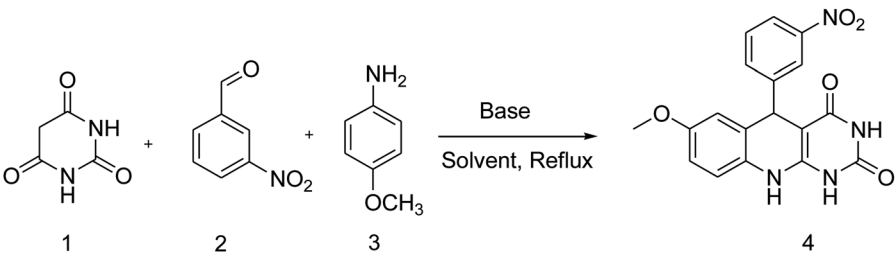


Fig. 5 XPS analysis for N(1.3 wt%)-MSN: (a) deconvolution of the Si 2p, (b) spectrum of N 1s.



Table 1 Optimization of the reaction conditions for the synthesis of arylpyrimido[4,5-*b*]quinolines^a


Entry	Solvent	Base	Temperature	Yield (%)
1	EtOH	—	Reflux	N. R.
3	EtOH	Et ₃ N (20 mol%)	Reflux	62
4	EtOH	L-Proline (20 mol%)	Reflux	65
5	H ₂ O	L-Proline (20 mol%)	Reflux	58
6	CH ₃ CN	L-Proline (20 mol%)	Reflux	52
7	EtOH	N(0.6 wt%)-MSN (20 mg)	Reflux	56
8	EtOH	N(1.3 wt%)-MSN (20 mg)	Reflux	70
9	EtOH	N(1.7 wt%)-MSN (20 mg)	Reflux	59
10	EtOH/H ₂ O (9 : 1) ^b	N(1.3 wt%)-MSN (20 mg)	80 °C	70
11	EtOH/H ₂ O (7 : 3) ^b	N(1.3 wt%)-MSN (20 mg)	80 °C	76
12	EtOH/H ₂ O (5 : 5) ^b	N(1.3 wt%)-MSN (20 mg)	80 °C	87
13	EtOH/H ₂ O (3 : 7) ^b	N(1.3 wt%)-MSN (20 mg)	80 °C	72
14	EtOH/H ₂ O (5 : 5) ^b	MSN (20 mg)	80 °C	N. R.
15	EtOH/H ₂ O (5 : 5) ^b	N(0.6 wt%)-MSN (20 mg)	80 °C	75
16	EtOH/H ₂ O (5 : 5) ^b	N(1.7 wt%)-MSN (20 mg)	80 °C	82
17	EtOH/H ₂ O (5 : 5) ^b	N(1.3 wt%)-MSN (20 mg)	70 °C	71
18	EtOH/H ₂ O (5 : 5) ^b	N(1.3 wt%)-MSN (20 mg)	90 °C	86

^a Reaction conditions: barbituric acid (1 mmol), 3-nitrobenzaldehyde (1 mmol) and 4-methoxy aniline (1 mmol) in 10 mL solvent at the reflux for 12 h. ^b Amounts of the applied volume for each solvent.

using 20 mg of every as-synthesized catalyst. It can be seen in entries 7–9 that N(1.3 wt%)-MSN shows a higher yield in EtOH. In the next step, using water as a co-solvent in the reaction medium was investigated. According to the obtained results, the volume ratio of 1 : 1 of H₂O/EtOH was better than that of absolute ethanol when N(1.3 wt%)-MSN was used (entry 12). It can be seen in entry 16 that the catalytic performance of N(1.7 wt%)-MSN was lower than that of N(1.3 wt%)-MSN. This could be related to increasing the basicity of the reaction medium during the synthesis of N-doped mesoporous silica nanoparticles, causing it to form the catalyst with different morphologies and catalytic activities.

To investigate the effect of temperature on the progress of the reaction, the catalytic activity of N(1.3 wt%)-MSN was studied at different temperatures. The obtained results showed that the catalyst exhibited more activity at 80 °C (entry 12).

Consequently, the as-synthesized N(1.3 wt%)-MSN composite showed the best yield (87%) in 10 mL H₂O/EtOH with a volume ratio of 1 : 1 at 80 °C (entry 12).

For extended studies on the catalytic activity of N(1.3 wt%)-MSN in the synthesis of arylpyrimido[4,5-*b*]quinolines, the reaction of barbituric acid (or thiobarbituric acid) and aniline and benzaldehyde derivatives was examined in the presence of 20 mg of the catalyst (Table 2). The reaction yields exactly prove

that the presence of electron-donating groups (such as methoxy) on aniline increases the yield of products, whereas the presence of electron withdrawing groups reduces the reaction yield. Also, benzaldehydes bearing electron withdrawing groups produced higher reaction yields and the presence of electron donating groups in the structures lead to lowering of the progress of the reaction. FTIR, ¹H NMR, and ¹³C NMR spectra of the as-synthesized products are presented in the ESI.†

Proposed mechanism

According to other similar works,²⁴ the following mechanism for the multicomponent synthesis of arylpyrimido[4,5-*b*]quinolone-dione is suggested (Scheme 2). It can be seen in Scheme 2 that the Knoevenagel condensation of barbituric acid and benzaldehyde in the presence of a basic catalyst (N(1.3 wt%)-MSN) resulted in the formation of intermediate **I**. Furthermore, the Michael addition of the aniline through a nucleophilic attack on structure **I** produced intermediate **II**. Subsequently, cyclocondensation and water removal in intermediate **III** afforded the desired product.

Reusability of the catalyst

Reusability of the heterogeneous catalysts was studied through subsequent runs. In this way, after the completion of the

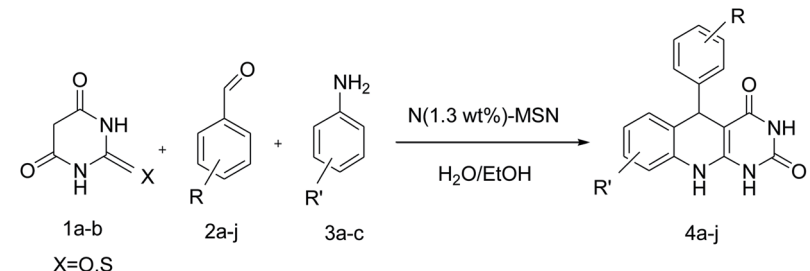
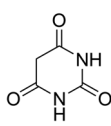
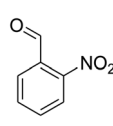
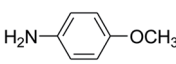
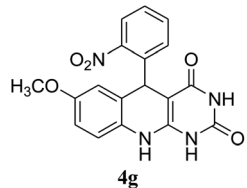
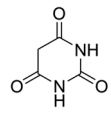
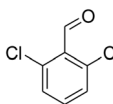
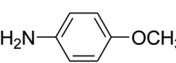
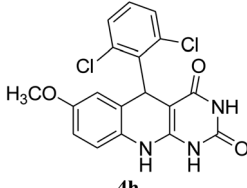
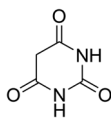
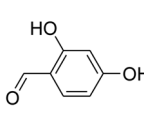
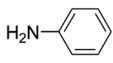
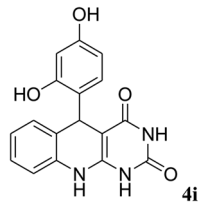
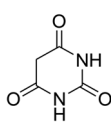
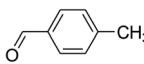
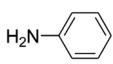
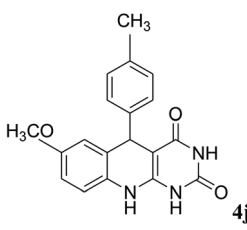
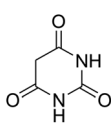
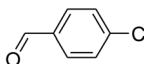
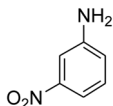
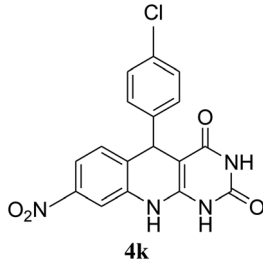


Table 2 Investigation of the catalytic activity of N(1.3 wt%)-MSN for the synthesis of some arylpyrimido[4,5-*b*]quinolone-dione derivatives^a

Entry	Time (h)	Dicarbonyl	Aldehyde	Aniline	Product	Yield ^b (%)
1	9					87/75/82 ^c
2	11					82
3	14					81
4	8					79
5	10					77
6	16					89



Table 2 (Contd.)

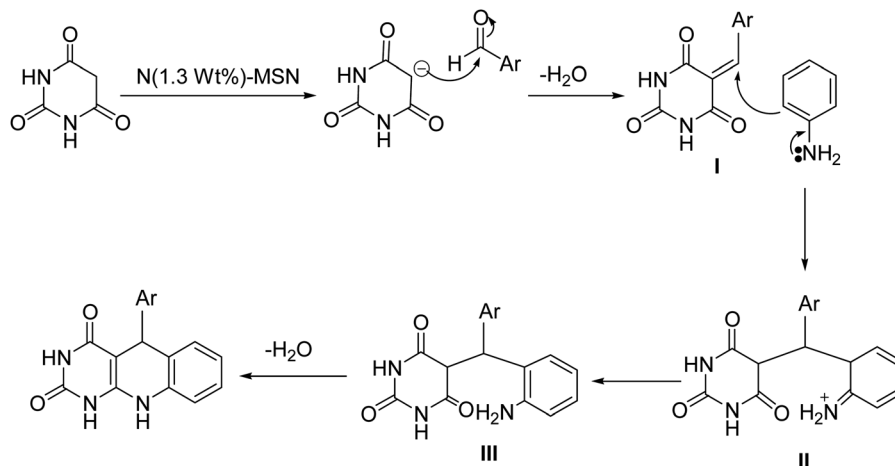
						
Entry	Time (h)	Dicarbonyl	Aldehyde	Aniline	Product	Yield ^b (%)
7	12				 4g	85
8	10				 4h	82
9	14				 4i	75
10	11				 4j	78
11	24				 4k	<20

^a Reaction conditions: dicarbonyl (1 mmol), aldehyde (1 mmol), aniline (1 mmol) in 10 mL EtOH/H₂O (5 : 5) in the presence of 20 mg N(1.3 wt%)-MSN at 80 °C. ^b Isolated yield. ^c Yield of product using N(0.6 wt%)-MSN and N(1.7 wt%)-MSN, respectively.

reaction, the solid base catalyst was separated using a magnetic field, washed with water and ethanol several times and applied once more in the same reaction. The obtained results exhibited

that there was no considerable change in the catalyst performance and yield of the desired product even after four cycles (Fig. 6).





Scheme 2 The suggested mechanism for the synthesis of arylpyrimido[4,5-*b*]quinolone-diones.

Experimental

Materials and methods

All of the chemicals were obtained from Sigma-Aldrich and Merck companies and used without further purification. To investigate the phase and crystalline structure of the as-synthesized catalysts, the N_2 adsorption/desorption analysis (BET) was employed to calculate the specific surface area of the obtained catalysts using an automated gas adsorption analyzer (Tristar 3000, Micromeritics) at -196°C . X-ray diffraction was performed using a Philips X'pert MPD diffractometer with a Cu operating at a current of 100 mA and a voltage of 45 kV, with the Cu-K α radiation ($\lambda = 0.154056\text{ nm}$) at the 2θ range of 10 – 80° and scanning at the speed of 0.05 degree per minute. The surface morphology of the as-prepared catalysts was studied using a Mira3-XMU field emission scanning electron microscope (FESEM) with a scanning electron electrode operating at 15 kV. The morphology of the N-doped mesoporous silica nanoparticles was observed using high-resolution TEM on a FEI Tecnai F20 USA microscope at an accelerating voltage of 200 kV. Also, to measure the amounts of nitrogen amount in the as-synthesized core shells, the elemental analysis was performed

by using a Carlo ERBA model EA 1108 analyzer. X-ray photoelectron spectroscopy (XPS) analysis was performed to prove the nitrogen doping into the silica structure using a Perkin Elmer RBD upgraded system (PHI-5000C ESCA) with Al/Mg-K radiation. FTIR spectra were recorded using the KBr pellet method in the range of 400 – 4000 cm^{-1} on a Perkin-Elmer 781 spectrophotometer, and an impact 400 Nicolet FTIR spectrophotometer was employed to assign the functional groups of the as-synthesized derivatives of 5-arylpyrimido[4,5-*b*]quinoline-diones. Furthermore, investigation on the structural confirmation of 5-arylpyrimido[4,5-*b*]quinoline-diones derivatives was carried out by ^1H NMR and ^{13}C NMR methods, which were performed in the DMSO- d_6 solvent on a Bruker DRX-400 spectrometer. The melting points of all 5-arylpyrimido[4,5-*b*]quinoline-diones derivatives were determined using an Electrothermal Mk3 apparatus.

Synthesis of magnetic nanoparticles

The synthesis of magnetic nanoparticles was performed following our previous work.¹ Initially, 0.0845 g $\text{FeCl}_2 \cdot 4\text{H}_2\text{O}$ and 0.2 g $\text{FeCl}_3 \cdot 6\text{H}_2\text{O}$ were dissolved into 50 mL of deionized water at 85°C . Then, 0.6 mL of ammonia was added to the obtained solution and stirred under the nitrogen atmosphere at 85°C for 30 min . After filtering, the resulting magnetic nanoparticles were washed with DI water and ethanol, and finally dried at room temperature.

Synthesis of core-shell magnetic mesoporous N-doped silica nanoparticles (N-MSN)

0.1 g of the as-prepared magnetic nanoparticles and 0.7 g CTAB (as a structural directing agent) were added to 160 mL of deionized (DI) water and sonicated for 10 min to form a good dispersion. Next, the mixture was added to 220 mL of ethanol comprising 1.2 mL of the NH_3 solution. Afterward, DEA as a source of nitrogen in different amounts (0.5 , 1.0 and 1.5 mL) was added in the solution. Then, the TEOS solution (0.4 mL TEOS in 10 mL ethanol) was added slowly to the mixture under stirring. The resultant solution was stirred for 12 h . Eventually,

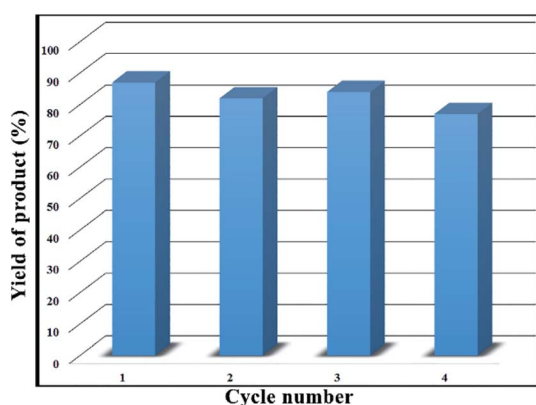


Fig. 6 Reusability of the N(1.3 wt%)-MSN catalyst in the multicomponent reaction.



the prepared magnetic solid was separated by a magnet and washed with ethanol several times. The attained solid was calcined in the furnace at 550 °C for 6 h (in an air atmosphere at a ramp rate of 5 °C min⁻¹) to eliminate the templates. So, the core-shell magnetic mesoporous N-doped silica nanoparticles were synthesized and labeled as N(x wt%)-MSN (x = the content of nitrogen in the core-shell magnetic mesoporous N-doped silica nanoparticles, as measured by the elemental analysis: 0.6, 1.3 and 1.7 wt%).

Synthesis of magnetic mesoporous silica nanoparticles (MSN)

To prepare the magnetic mesoporous silica nanoparticles (or, namely, MSN), all the procedures were followed as per the above-described method. However, the difference was that DEA was not used. The synthesized solid was named as MSN.

Catalyst performance for the synthesis of arylpyrimido[4,5-*b*]quinoline derivatives

For preparing the arylpyrimidoquinoline derivatives, 1 mmol of aniline derivatives, 1 mmol of barbituric acid and 1 mmol of benzaldehyde in the presence of 20 mg of the synthesized catalyst in water and ethanol solvents (at a volumetric ratio 1 : 1 at 80 °C) were reacted. The reaction progress was monitored by TLC, and after the completion of the reaction, the magnetic catalyst was removed from the reaction medium by a magnet. Furthermore, the obtained precipitate was filtered and washed with cold ethanol and water and the structure of the product was fully confirmed with FTIR, ¹H NMR and ¹³C NMR data.^{24,36,37}

Conclusion

In this study, mesoporous magnetic N-doped silica nanoparticles as a heterogeneous basic catalyst (N(x wt%)-MSN) was prepared. In the presented process, DEA was used as a nitrogen source and TEOS as a silica precursor. The as-prepared catalyst was applied successfully for the synthesis of some arylpyrimido[4,5-*b*]quinoline-dione derivatives in high yields. The nitrogen doping by this method is a new route for developing highly efficient solid base catalysts.

Conflicts of interest

There are no conflicts to declare.

Acknowledgements

The Research Council of Kashan University should be appreciated for supporting this work.

References

- 1 S. Neamani, L. Moradi and M. Sun, *Appl. Surf. Sci.*, 2020, **504**, 144466.
- 2 E. G. Derouane and S. M. Roberts, *Microporous and mesoporous solid catalysts*, John Wiley & Sons, 2006, pp. 171–187.
- 3 W. Bing, L. Zheng, S. He, D. Rao, M. Xu, L. Zheng, B. Wang, Y. Wang and M. Wei, *ACS Catal.*, 2018, **8**, 656.
- 4 H. Hattori, *Chem. Rev.*, 1995, **95**, 537.
- 5 F. Hoffmann, M. Cornelius, J. Morell and M. Fröba, *Angew. Chem.*, 2006, **45**, 3216.
- 6 A. L. de Lima, C. M. Ronconi and C. J. A. Mota, *Catal. Sci. Technol.*, 2016, **16**, 2877.
- 7 J. L. Paris, M. V. Cabañas, M. Manzano and M. Vallet-Regí, *ACS Nano*, 2015, **9**, 11023.
- 8 W. Xie, L. Hu and X. Yang, *Ind. Eng. Chem. Res.*, 2015, **54**, 1505.
- 9 C. H. Tsai, M. Xu, P. Kunal and B. G. Trewyn, *Catal. Today*, 2018, **306**, 81.
- 10 X. Liu, D. Chen, L. Chen, R. Jin, S. Xing, H. Xing, Y. Xing and Z. Su, *Chem.-Eur. J.*, 2016, **22**, 9293.
- 11 Y. Huang, *Functionalization of mesoporous silica nanoparticles and their applications in organo metallic and organometallic catalysis*, Univ. Iowa State, 2009, p. 1.
- 12 Z. Tian, Y. Xu and Y. Zhu, *Mater. Sci. Eng., C*, 2017, **71**, 452.
- 13 Z. A. Allothman, *Materials*, 2012, **5**, 2874.
- 14 I. A. Rahman, M. Jafarzadeh and C. S. Sipaut, *Ceram. Int.*, 2009, **35**, 1883.
- 15 J. J. Lin, P.-Y. Hsu, Y. L. Wu and J. J. Jhuang, *Sensors*, 2011, **11**, 2796.
- 16 J. Liang, Z. Liang, R. Zou and Y. Zhao, *Adv. Mater.*, 2017, **29**, 1701139.
- 17 K. Sugino, N. Oya, N. Yoshie and M. Ogura, *J. Am. Chem. Soc.*, 2011, **133**, 20030.
- 18 T. Hasegawa, C. K. Krishnan and M. Ogura, *Microporous Mesoporous Mater.*, 2010, **132**, 290.
- 19 S. Ernst, M. Hartmann, S. Sauerbeck and T. Bongers, *Appl. Catal., A*, 2000, **200**, 117.
- 20 A. Shahzeydi, M. Ghiaci, L. Jameie and M. Panjepour, *Appl. Surf. Sci.*, 2019, **485**, 194.
- 21 N. M. Nursam, X. Wang, J. Z. Y. Tan and R. A. Caruso, *ACS Appl. Mater. Interfaces*, 2016, **8**, 17194.
- 22 S. M. Sadeghzadeh and M. A. Nasser, *Catal. Today*, 2013, **217**, 80.
- 23 C. Zhang, H. Wang, F. Liu, L. Wang and H. He, *Cellulose*, 2013, **20**, 127.
- 24 A. Khalafi-Nezhad, S. Sarikhani, E. S. Shahidzadeh and F. Panahi, *Green Chem.*, 2012, **14**, 2876.
- 25 R. Daoud, J. Desneves, L. W. Dedy, L. Tilley, R. J. Scheper, P. Gros and E. Georges, *Biochemistry*, 2000, **39**, 6094.
- 26 T. Suzuki, N. Fukazawa, K. San-nohe, W. Sato, O. Yano and T. Tsuruo, *J. Med. Chem.*, 1997, **40**, 2047.
- 27 R. Klingenstein, P. Melnyk, S. R. Leliveld, A. Ryckebusch and C. Korth, *J. Med. Chem.*, 2006, **49**, 5300.
- 28 A. Lilienkampf, J. Mao, B. Wan, Y. Wang, S. G. Franzblau and A. P. Kozikowski, *J. Med. Chem.*, 2009, **52**, 2109.
- 29 A. B. A. El-Gazzar, H. N. Hafez and G. A. M. Nawwar, *Eur. J. Med. Chem.*, 2009, **44**, 1427.
- 30 H. I. Ali, K. Tomita, E. Akaho, H. Kambara, S. Miura, H. Hayakawa, N. Ashida, Y. Kawashima, T. Yamagishi and H. Ikeya, *Bioorg. Med. Chem.*, 2007, **15**, 242.
- 31 X. Li, X.-H. Zhu, Y. Fang, H.-L. Yang, X. Zhou, W. Chen, L. Jiao, H. Huo and R. Li, *J. Mater. Chem. A*, 2014, **2**, 10485.



- 32 L. W. Lin and Y. H. He, *CrystEngComm*, 2012, **14**, 3250.
- 33 G. Polzonetti, C. Battocchio, G. Iucci, M. Dettin, R. Gambaretto, C. Di Bello and V. Carravetta, *Mater. Sci. Eng., C*, 2006, **26**, 929.
- 34 A. A. Razzaq, Y. Yao, R. Shah, P. Qi, L. Miao, M. Chen, X. Zhao, Y. Peng and Z. Deng, *Energy Storage Materials*, 2019, **16**, 194.
- 35 X. Song and L. Gao, *Langmuir*, 2007, **23**, 11850.
- 36 M. H. Mosslemin, E. Zarenezhad, N. Shams, M. N. S. Rad, H. Anaraki-Ardakani and R. Fayazipoor, *J. Chem. Res.*, 2014, **38**, 169.
- 37 C. Verma, L. O. Olasunkanmi, I. B. Obot, E. E. Ebenso and M. A. Quraishi, *RSC Adv.*, 2016, **6**, 15639.

